The Things You Can't Ignore: Evolving a Sub-Arcsecond Star Tracker

John Enright
Department of Aerospace Engineering, Ryerson University
350 Victoria St, Toronto, Ontario, M5B 2K3; 416-979-5000(x4174)
jenright@ryerson.ca

Doug Sinclair
Sinclair Interplanetary
268 Claremont St. Toronto, Canada; 647-286-3761
dns@sinclairinterplanetary.com

Tom Dzamba
Department of Aerospace Engineering, Ryerson University
350 Victoria St, Toronto, Ontario, M5B 2K3; 416-979-5000(x4973)
tdzamba@ryerson.ca

ABSTRACT

The feasibility of a star tracker with 1 arc-second accuracy and 1 deg/sec slew capability is explored, using the ST-16 design as a starting point. Whole-sky simulation is used to determine the impact of optical design on the star tracker availability. The current optical calibration process is examined, and shown to be inadequate for the desired performance. Additional factors that become important at high accuracy are examined. These are detector calibration, temperature variation, chromatic aberration, stellar aberration and proper motion. Plausible methods of dealing with each of these are presented.

OVERVIEW

The S3S development project has produced the ST-16 star tracker, a tiny integrated design intended for small satellites. It has been successful in the marketplace, and flight units have been delivered for a number of astronomical and Earth-observing missions. Ground-based testing supports an accuracy claim of 7 arc-seconds cross-axis, and 2-3 arc-second performance is expected once above the atmosphere. The first orbital data (expected late 2012) should validate this.

There is demand, particularly from the Earth-observing community, for a higher accuracy star tracker. In this paper we look at target requirements of:

- 1 arc-second (i.e., ~ 4.8 μrad) accuracy, while slewing at
- 1 deg/sec (to track a target on the Earth's surface from LEO), with
- 99% availability of a robust attitude fix.

We try to answer the question: what modifications must be made to the standard ST-16 to meet these requirements? In particular, what subtle effects are we ignoring at the moment which we must consider in detail when we move to higher accuracy? Armed with this information, we can prioritize our technical development and identify key technical risks.

OPTICAL TRADES

We begin by examining the optical design of the ST-16, and looking at its performance and sources of error. We then investigate whether better performance could be achieved with better optics. Our primary optimization is to look for valid optical designs by changing $F_{\#}$ and D. The validity of a design is influenced two primary factors: availability and accuracy. Availability indicates the fraction of the sky where a good attitude fix is possible. Accuracy considers the expected accuracy of the sensor for a given optical design. Given requirements for these two metrics, we can identify regions of the optical design space where performance will meet our requirements.

Signal-to-Noise Calculations

An analytical understanding of signal-to-noise will be essential to the trades which will follow. The number of photo-electrons from a single star is given by:

$$S_e = \eta_Q t_e A \phi_0 \cdot 10^{\frac{-2}{5}(m_1 - m_0)} \tag{1}$$

where η_Q is the mean quantum efficiency of the detector; t_e, is the observation of time; A, the aperture area; ϕ_0 the stellar flux from a reference star; and m_1, and m_0 the visual magnitudes of both the star in question and the reference star. Following Reed[1] and making judicious assumptions about stellar type and wavelength band, we use $\phi_0 = 1.8 \times 10^{10}\, m^{-2} s^{-1}$ (for AM0 measurements) for a magnitude zero star. Incorporating this change and expressing A in terms of the aperture diameter, D, give:

$$S_e = \frac{1}{4}\eta_Q t_e \pi D^2 \phi_0 \cdot 10^{-\frac{2}{5}m_1} \tag{2}$$

The noise during the readout is a function of the number of pixels included in the star image. Assuming a rotationally symmetric static point-spread function, of radius, ρ(in pixels), and pixel size, γ, we can calculate the number of pixels that contribute noise. If the sensor is not moving, this is:

$$M_{static} = \pi \rho^2 \tag{3}$$

When motion is present we must consider the length of the track on the detector. This is a function of the focal length of the lens system. In terms of the $f-$number of the lens, $F_\#$, the focal length is:

$$f = F_\# D \tag{4}$$

Considering only cross-boresight motion, for the present, the total track length, δ (in pixels), during the exposure is:

$$\delta = \frac{f \tan(\omega t_e)}{\gamma} = \frac{F_\# D \tan(\omega t_e)}{\gamma} \tag{5}$$

The total number of pixels in the PSF is therefore:

$$M_{total} = \pi\rho^2 + 2\rho\delta = \pi\rho^2 + 2\rho\frac{F_\# D \tan(\omega t_e)}{\gamma} \tag{6}$$

Translating the number of pixels into an expected noise depends on the dominant noise sources. The regime where we are using the MT9P031 seems only weakly dependent on exposure time. This suggests that we are dominated by read-noise. Neglecting the weak time dependence we can write the expected noise standard deviation as:

$$N_e = \sqrt{M_{total}}\sigma_{e^-} \tag{7}$$

This leads to an expression for the expected signal to noise ratio, R:

$$R = \frac{\eta_Q t_e \pi D^2 \phi_0 \cdot 10^{-\frac{2}{5}m_1}}{4\sigma\left(\pi\rho^2 + \rho\frac{2F_\# D \tan(\omega t_e)}{\gamma}\right)^{1/2}} \tag{8}$$

To achieve a specified target, SNR, R_t, we can solve for the corresponding cutoff magnitude, m_t:

$$m_t = -\frac{5}{4}\log_{10}\left(\frac{\rho\left(\pi\rho\gamma + 2F_\# D\tan(\omega t_e)\right)R_t^2\sigma^2}{\gamma\left(\eta t \pi D^2 \phi_0\right)^2}\right)$$

Thus, stars of this magnitude or brighter should always be detectable.

Estimating Availability

In order to assess the raw availability of a particular sensor design, we must combine the SNR results with a survey of the sky and an estimate of the FOV bounds. For simplicity we will consider a circular FOV, with angular radius, θ, determined by the minor axis of the detector, h. The extent of the FOV is determined by the optical design of the system:

$$\theta = \arctan\frac{h}{2f} = \arctan\left(\frac{h}{2DF_\#}\right) \tag{9}$$

We generate an (approximately) even distribution of boresight directions using a Generalized Spiral[2]. For each location we evaluate the number of visible stars that are brighter than the current magnitude limit, and lie within θ of the boresight. In order to optimize our storage requirements, we classify views as having either:

- Less than two visible stars. Matching and tracking are impossible.

- Exactly two visible stars. Tracking possible (but not implemented by current S3S), matching impossible.
- Exactly three visible stars. Tracking possible, minimum observation for matching.
- Four or more stars. Good conditions for both matching and tracking.

Depending on the final operating conditions, the assumptions behind the three and four-star categories may need further study. If enough of the star triangles are ambiguous, four-star scenes may represent the minimum number for reliable matching. At present, we do not assess triangle ambiguity in the availability calculations.

Estimating Accuracy

Assuming that a particular star-field can be matched against the star tracker's on-board catalog, the accuracy of the resulting attitude solution is closely related to the accuracy in relating a star image on the focal plane to a star vector in space. For the existing ST-16 hardware, the star-vector's angular uncertainty, σ_θ, is approximately 27.6 μrad. This is a combination of centroiding error on the detector, and modelling error in the optics. We can postulate that the corresponding error in the centroid location, σ_p, is independent of focal length.

The overall sensor accuracy, σ_S is affected by the accuracy of the individual star vectors, as well as the distribution of vectors within the field of view. This complex dependency makes results difficult to generalize. Instead, we adopt a less rigourous approach and assume that the cross-boresight accuracy is approximated by

$$\sigma_S = \frac{1}{\sqrt{N_S}}\sigma_\theta \tag{10}$$

where N_S is the number of stars, in the limiting solution case (typically 2,3, or 4). In many star trackers, the roll accuracy (i.e., round the boresight), is 5-10 times worse than the boresight accuracy.

Optical Trade Results

We can search for candidate optical designs by evaluating the above metric calculations for different lens combinations. Here we present preliminary results from this simulation. The defining parameters are given in Table 1, and are based on the current ST-16 detector. We also include an alternative detector, the CMOSIS CMV4000.

Table 1: Optical Trade Study Detector Parameters

Parameter	MT9P031	CMV4000
h(mm)	4.28	11.3
η_Q	0.5	0.5
ρ	3	3
t_e (s)	0.1	0.1
γ (μm)	2.2	5.5
σ_e	3.5	13
R_t	50	50
ω(°/s)	1	1

The CMV4000 is a 1-inch format detector. The per-pixel noise from this detector is higher, but the larger area allows us to use larger optics at lower values of $F_\#$.

We make the following notes about the selection of these parameters:

- The SNR value $R_t$was chosen so that the predicted threshold magnitude for the current ST-16 design matched our field results.
- The angular rate, ω is chosen to allow satellite body tracking of a ground target from LEO.

Results from the trade studies are shown in Figure 1 – Figure 2. These plots show contours of availability for different optical designs. The current S3S optical design is located near the bottom left of the figures ($F_\# = 1.2,\ D = 12\text{mm}$). The availability contours in these figures all show similar trends. Unsurprisingly faster optics (i.e., lower values of $F_\#$), have larger FOV and can thus see more stars. It is more interesting to observe the variation with D. Although larger apertures collect more photons, increasing D at constant $F_\#$ increases f, shrinking the size of the FOV. As the FOV shrinks, fewer stars will be visible around any given boresight direction. Additionally, the interaction between the shrinking FOV and the sensor motion will increase the streak length of each star on the detector, increasing the integrated noise. We see that the star population distribution favours increasing the stars in view by increasing θ rather than merely detecting dimmer stars.

These figures show that using the lowest possible $F_\#$ is key. The baseline ST-16 uses a $F_\# = 1.2,\ D = 12\text{mm}$ lens. If the larger CMV4000 detector is chosen, commercial lenses at $F_\# = 1.4,\ D = 40\text{mm}$ and $F_\# = 0.9,\ D = 52\text{mm}$ have been identified which may be suitable.

Table 2 shows four reference designs based on various lens and detector combinations. Design-1 is very close to

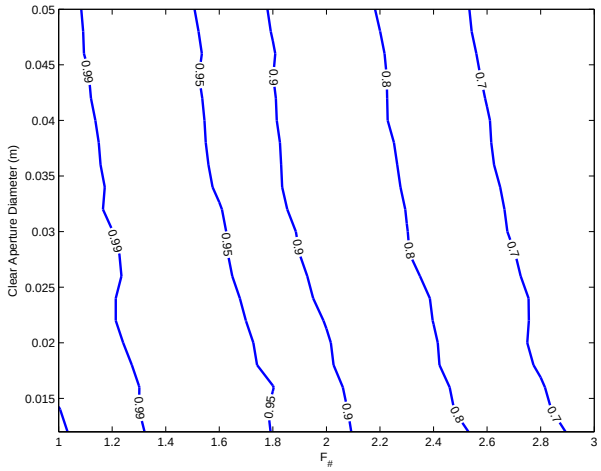

Figure 1: Trade study results from MT9P031 detector (Two-Star).

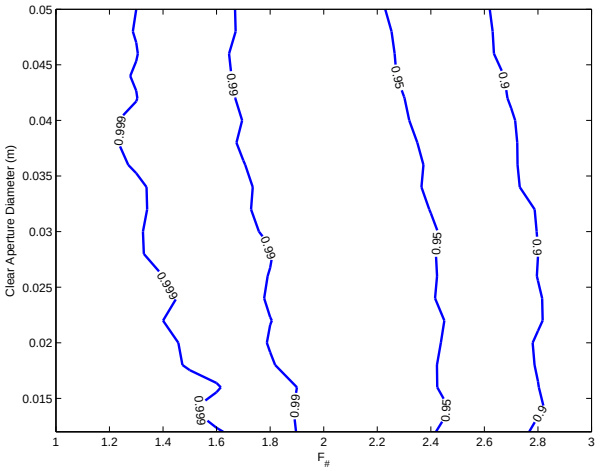

Figure 3: Trade study results from CMV4000 detector (Two-Star).

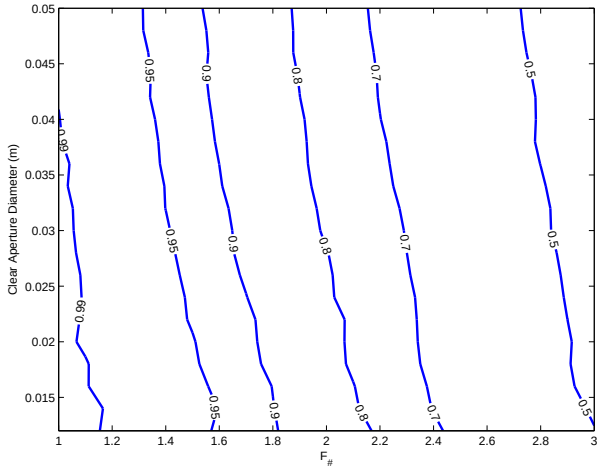

Figure 2: Trade study results from MT9P031 detector (Three-Star).

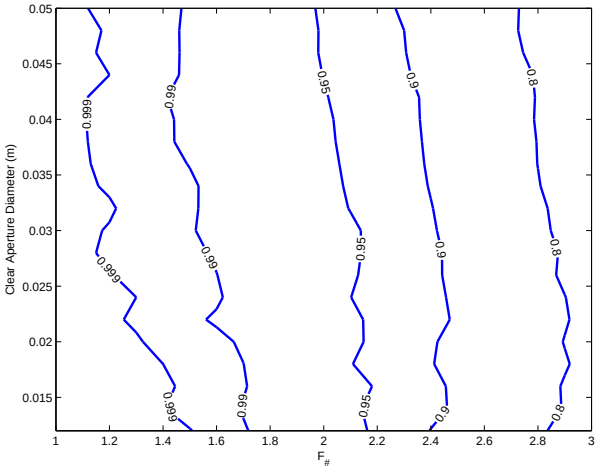

Figure 4: Trade study results from CMV4000 detector (Three-Star).

the baseline ST-16 configuration (the analysis is slightly different, so the specifications are not precisely the same). Design-2 is the same Aptina detector and a (hypothetical) faster lens. Design-3 and Design-4 represent the CMOSIS detector, combined with the lenses described above. Our two ST-16 derived designs are attractive due to the heritage they exploit, but require substantial refinement in the star centroid determination. The latter concepts theoretically meet our specifications, but require more extensive redesign of the sensor hardware. Regardless of the final sensor configuration, improvements in the calibration, and hence σ_θ, specifications will be necessary.

One factor not yet discussed is the role of accuracy. Sensor accuracy depends on the centroid accuracy, σ_P, which in turn, depends on the calibration effectiveness and the effects of temporal noise. Figure 5 and Figure 6 show the total error from these sources (in pixels) required to meet the accuracy specification of $\sigma_S = 4.8\,\mu\text{rad}$. The Aptina point designs are found in the bottom left, and the CMOSIS designs in the top left of the corresponding figures. Comparing the two detectors, the error requirements are quite similar; $\sigma_P \approx 0.07$ pixels will meet the accuracy target. Thus, we must improve centroid accuracy about three-fold over the ST-16. From a comparison of Figure 2 and Figure 5 we do not see any regions where a lens change, *without* an improvement in σ_P will meet both the accuracy and availability requirements. The ease with which we can achieve the target centroid error with the CMV4000 depends on the effects of pixel size. At present the relation between γ and σ_P is not clear.

Table 2: Reference Designs

Parameter	Design-1	Design-2	Design-3	Design-4
Detector	Aptina MT9P031	Aptina MT9P031	CMOSIS CMV4000	CMOSIS CMV4000
$F_{\#}$	1.2	1.0	1.4	0.95
D (mm)	12	12	40	52
θ (°)	7.5	10.1	5.7	6.4
m_t	5.9	6.0	6.9	7.5
Catalog Size ($\times 10^3$)	4.5	5.1	13.8	25.7
Availability (3-star)	0.9804	.9988	0.9921	0.9999

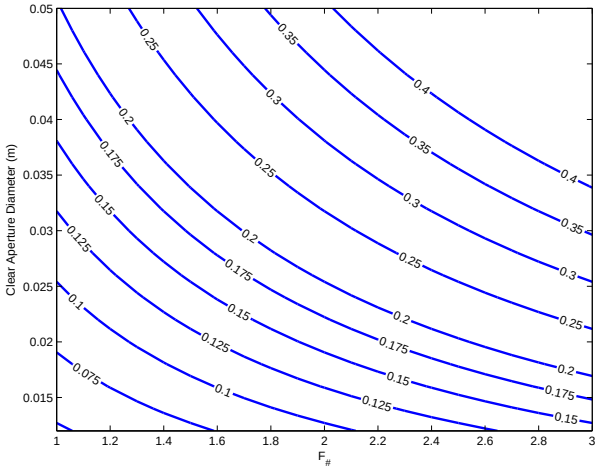

Figure 5: Calibration residual requirements, in pixels, for MT9P031.

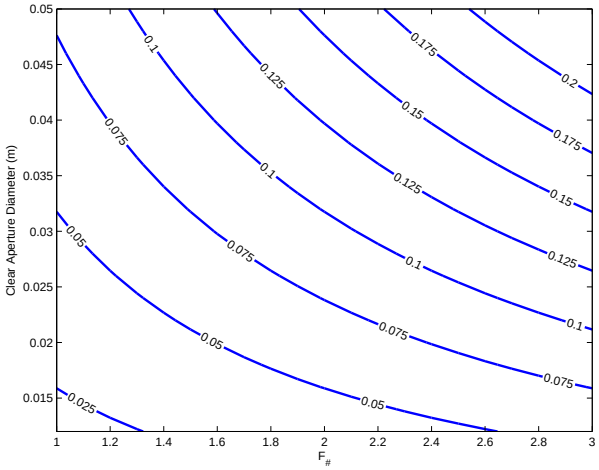

Figure 6: Calibration residual requirements, in pixels, for CMV4000.

INCREASING ACCURACY

If we cannot increase accuracy by simply changing the lens, what can we do to achieve the target requirements? The driving parameter is the error in relating a star image to a star vector, σ_θ. There are a number of ways in which this can be done, all of which demand further study. It is not clear at this moment which error source dominates, and thus which problem to tackle first.

Detector Characterization

The pixels in the star tracker's detector are not all identical. There are two important effects: fixed pattern noise and gain variation. Both of these lead to error when determining the centroid of a defocused star image. It is possible to fully characterize a detector in the laboratory, and have the star tracker correct each image in real time. Unfortunately, the pixels may further change on-orbit in response to radiation damage.

Ideally the star tracker would incorporate a shutter and a calibration lamp, allowing the detector to be re-characterized periodically on-orbit. Where this is impossible, for reasons of mass and cost, it may be possible to estimate the state of each pixel over time by computational power alone, continually comparing the image seen to the expected image of the sky given the known attitude quaternion. Periodic spacecraft slews to image uninhabited regions of the Earth at night may serve as a proxy for a shutter.

Improved Detector

The MT9P031 detector used in the ST-16 was ideal for the original low-power, rapid-development design. However, it may not be the very best choice for a very accurate star tracker. A physically larger detector would allow the use of a larger f lens for an equivalent FOV. The effect of this

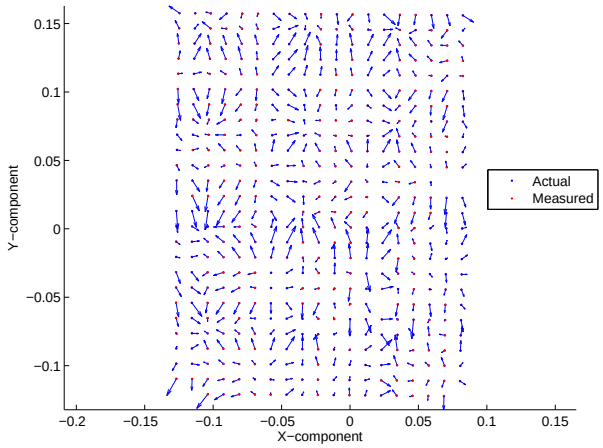

Figure 7: Typical residual error structure from S3S calibration.

on σ_θ is currently under study.

A detector with better stability under radiation damage than the MT9P031 is certainly desirable. This might allow a device to be fully characterized in the laboratory without requiring re-characterization on-orbit. The CMOSIS CMV4000 may be a good candidate for this.

Optical Calibration

Optical calibration allows us to associate a centroid location on the detector with an external direction vector. A combination of physical (e.g., focal length) and curve-fit (e.g., distortion coefficients) parameters is often necessary. As discussed in previous sections, improving calibration performance will be critical to the success of our high-accuracy design. We must consider modifications to both the mathematical framework for calibration as well as the procedures used to perform the calibration itself

The current approach used with the S3S is a 17 parameter fit adapted from Heikkela and Silven[3]. Our current residual error after calibration is equivalent to approximately 0.2 pixels or 0.44 μm. As calibrations go, this result is modest — Rufino and Accardo[4] report 0.01 pixel centroid error as their starting point (we acknowledge that they are concerned more with noise and centroid calculation, rather than the calibration of the whole camera). Examining a plot of the post-calibration residuals (Figure 7), shows clear evidence systematic effects. Higher order calibration terms can likely be used to remove the structure apparent in the error. Chromatic corrections may also be necessary Such corrections can be applied after the stars have been identified.

Laboratory calibration and validation presents a challenge for a high-accuracy star tracker. Our current approach employs a collimated point-source and a motorized test stand. This apparatus has a repeatability of 35 μrad, which is comparable to the residual calibration error. Thus, we are effectively at the accuracy limit of our current infrastructure. Moving to a high-accuracy design will require a change in approach or a significant investment in test equipment. One technique that shows promise is to perform a best-effort laboratory calibration and remove any residual errors by analyzing actual star images. Saamen, et al.[5], have proposed techniques for on-orbit star tracker calibration, and such an algorithm could be used on a revised design. Ground-based validation will still be somewhat tricky because relative refraction will cause distortions on the order of 15 μrad across the sensor FOV, even when pointed at zenith.

EFFECTS WE CAN NO LONGER IGNORE

Once the centroid measurement error (i.e., σ_θ), of the star tracker has been brought to ~ 4.8 μrad, the overall accuracy of the system begins to be limited by a host of subtle effects that have been ignored in the existing ST-16 design. These must be addressed before further accuracy gains can be achieved.

Chromatic aberration

Chromatic aberration is a property of refractive optical systems, whereby the effective focal length varies slightly as a function of the wavelength of the incoming light. An incoming ray of white light will appear on the focal plane as a coma-shaped rainbow, red at one end and blue at the other. A monochrome detector will see the coma shape, but will not be able to distinguish any colour information.

The aberration is significant because different stars have different surface temperatures and thus different dominant colours. A hot (blue) star will produce a different centroid pixel location on the detector than a cool (red) star in the same position in space. This leads to uncertainty in the true star vector.

A high accuracy star tracker can take one of two approaches. Chromatic aberration can be eliminated from the optics, or compensated for in software. Refractive optics can be made almost achromatic by careful selection of glasses, and/or with a bandpass filter. Purely reflective optics are inherently achromatic, but they suffer from coma aberration in wide angle designs.

Chromatic compensation requires that the star tracker's on-board catalog carries spectral information for each star. Once a star is identified, a colour-dependent

correction term can be applied to move its centroid slightly before the final solution is computed. Partial compensation can be achieved simply by flagging unusually red or blue stars in the catalog with a "do not use" bit.

Thermal Deformation

Temperature changes caused by the space environment may alter the optical parameters of a star tracker. Here we consider two effects: change in bulk temperature of the entire star tracker, and temperature gradients from one side of the star tracker to another.

Changes in the bulk temperature of an optical system cause thermal expansion in the glass lens elements, and in the metal structure that positions them. It also causes changes in the index of refraction of the glass itself. The aerial photography community is increasingly using commercial DSLR cameras for mapping, and this has lead to some studies on the effects of bulk temperature. One experiment on a 20 mm lens shows a change in focal length of +30 ppm/C[6]. Another experiment on a 28 mm lens shows a rate of +35 ppm/C[7]. It is not known how directly DSLR lens results can be related to the smaller video lenses that we use.

Lateral temperature gradients across a cantilever lens assembly will result in bending. Consider a simplified lens structure consisting of a black anodized aluminum tube 20 mm in inner diameter and 10 mm long, with 1 mm wall thickness. Analysis shows that when illuminated from the side by sunlight there will be a temperature gradient of 1 C between the hot and cold sides. It will bend by a total of 12 μrad . Physically larger lenses will experience much greater temperature gradient and bend angle.

The change in focal length due to bulk temperature changes will be noticeable, but correctable. Assume the rate is +35 ppm/C, and the lens operates 20 C from its design temperature. A star at the edge of the 7.5° FOV will appear to move by 92 μrad. So long as the star tracker can still correctly match the stars, it can then use the observed star positions to determine its effective focal length. While the current ST-16 does not correct for changing focal length, experiments show that it will reliably match at elevated temperatures.

The effect of bending a complex stack of optical elements is not easy to model, so here we shall consider a simple thin-lens system. The ray corresponding to a given pixel detector moves by half of the lens tube bend angle. There is nothing inherent in the image that would allow for the bend angle to be measured and corrected. Instead, the design must minimize the thermal gradient bending of the optics. The best way to do this is by enveloping the star tracker lens and housing under a baffle which has good circumferential thermal conductivity and has a separate thermal path to the spacecraft structure.

Table 3: Star Density near High-Parallax Stars (7.5° FOV, 5.75 Mag.)

Star Name	HD Number	No.of Neighbours
Alpha Centauri	128620/128621	29
Sirius	48915	26
61 Cygni	201091/201092	29
Lacaille 8760	202560	17
Lalanda 21185	95735	18
Groombridge 34	1326	21
Epsilon Eridani	22049	16
Procyon	61421	15
Tau Ceti	10700	14
Kapteyn's Star	33793	9
Epsilon Indi	209100	11
Lacaille 9352	217987	15
Sigma 2398	173739/173740	19

Star Positions

In low precision star trackers, it is reasonable to treat the star catalog as static. For higher accuracy calculations, we must consider three effects that can change the apparent star positions: Annual parallax, proper motion, and stellar aberration. *Annual parallax* is the angular motion caused by the Earth's motion about the sun — nearby stars will move slightly over six months. The second factor that must be accounted for is *proper motion,* i.e., the effect of secular motion of the stars themselves. Finally, *stellar aberration* is an angular displacement caused by the velocity of the observer. For each factor, we examine how it will affect sensor accuracy.

Parallax will have the smallest effect on sensor design. From Burnham[8], only 13 stars brighter than magnitude 9.0 have parallax exceeding 1.25 μrad — even α-Cen is only 3.61 μrad. None of the affected stars are in regions of the sky with poor star density (see Table 3) , so we may even choose to omit these stars from the catalog altogether.

Proper motion is an effect that can no longer be ignored in a high precision star tracker. Table 4 shows the distribution of annual motions for the S3S catalog. Clearly, maintaining our accuracy performance goals will require a correction to the cataloged star positions. Calculating this correction is simple, but does rely on knowl-

Table 4: Proper Motion Distribution

Proper motion (μrad/yr)	Mag. < 5.75	Mag. < 7.4
< 0.5	2942	21096
$0.5 - 1.0$	561	1956
$1 - 2$	212	749
$2 - 5$	87	249
$5 - 10$	28	46
$10 - 20$	9	11
$20 - 30$	2	3
$30 - 42$	0	2

edge of the absolute time.

The simplest correction for proper motion would be to exclude high-motion stars from the matching process. If we set this threshold at 1 μrad — allowing 5 μrad of motion over a 5 year mission lifetime — this would exclude about 9% and 4.4% of the stars from the two catalogs. This will likely impact availability in star-poor regions of the sky. Therefore we expect that some accommodation for proper motion will be necessary for satisfactory matching performance. Possible implementations could include correction factors for the tabulated triangles, or a periodic on-line regeneration of the whole triangle table.

The effects of stellar aberrations arise from the motion of the earth around the sun ($\sim$ 100 μrad) as well as the satellite around the earth ($\sim$ 25 μrad in LEO)[9]. If uncorrected, the former effect will result in a slow bias drift over the span of a year, and might be tolerable in some missions. The latter effect is much faster, and remains large enough to violate our accuracy targets. Shuster[10] provides analysis and corrections for the effects of aberrations. These corrections must be performed on a per-star basis but require relatively little computation. An additional consequence of stellar aberration is that the star tracker must now be provided with enough ephemeris information to calculate its orbital corrections.

The corrections necessary to maintain attitude accuracy in the presence of star position distortion are well understood. With a star match, orbital ephemeris, and global time information, we can remove most of these effects with little computational cost.

CONCLUSION

The impact of optical design on star tracker availability is well understood. Given an availability and slew rate requirement, and known detector properties, the legal optical parameters are constrained. This largely drives the F/#, though the focal length is also impacted.

The effect of optical design on accuracy is less clearly understood. Larger apertures are intuitively beneficial, but their quantitative effect together with physically larger detectors are not known. From a product perspective, larger apertures are expensive in terms of mass, volume, baffle and thermal control.

Our laboratory optical calibration equipment is challenged by the current work. Higher accuracy star trackers will need to self-calibrate on-orbit, using known star patterns to model their own optics. Continual self-calibration will help to correct for dimensional changes over time, be they caused by thermal expansion or structural warping. It appears that the current S3S operating paradigm of carrying minimal state information from frame to frame must be modified to allow for evolving long-term model estimates.

The ability to characterize the detector on-orbit is valuable. Adding a shutter is probably not something that will be done in the near term, for reasons of cost and reliability. A test lamp, which could be as simple as an LED on the circuit board, will be considered for future designs. Even without a shutter, the lamp should allow the gain of each pixel to be computed.

Stellar aberration and proper motion can be corrected, provided the star tracker has access to an accurate real-time clock and orbital ephemeris information. Again, the S3S concept of minimal interaction with the host spacecraft must be relaxed to allow a tighter coupling with the rest of the flight software. This loss of simplicity appears to be an inevitable consequences of the desire for greater accuracy.

In a few months, once the ST-16 is flight-proven, the team will be looking for a fresh challenge. The development of an arc-second star tracker seems to be feasible, and the product is in market demand. Time will tell whether we are successful.

References

1. Reed, B. C., "Education Notes/Rubrique Pédagogique- Stellar Magnitudes and Photon Fluxes," *Journal of the Royal Astronomical Society of Canada*, Vol. 87, April 1993, pp. 123.

2. Saff, E. and Kuijlaars, A., "Distributing many points on a sphere," *The Mathematical Intelligencer*, Vol. 19, No. 1, Dec. 1997, pp. 5–11.

3. Heikkila, J. and Silven, O., "A four-step camera calibration procedure with implicit imagecorrection," *1997 IEEE Computer Society Confer-*

ence on Computer Vision and Pattern Recognition, 1997. Proceedings., 1997, pp. 1106–1112.

4. Rufino, G. and Accardo, D., "Enhancement of the centroiding algorithm for star tracker measure refinement," *Acta Astronautica*, Vol. 53, No. 2, July 2003, pp. 135?147.

5. Samaan, M. A., Griffith, T., Singla, P., and Junkins, J. L., "Autonomous on-orbit calibration of star trackers," *Core Technologies for Space Systems Conference (Communication and Navigation Session)*, 2001.

6. Merchant, D., "Influence of Temperature on Focal Length for the Airborne Camera," San Antonio Texas, Nov. 2006.

7. Smith, M. and Cope, E., "The Effects of Temperature Variation on Single-Lens-Reflex Digital Camera Calibration Parameters," *International Archives of Photogrammetry, Remote Sensing and Spatial Information Sciences*, Vol. XXXVIII, Part 5, Newcastle upon Tyne, UK.

8. Burnham, R., *Burnham's celestial handbook: an observer's guide to the Universe beyond the solar system*, Vol. 1, Dover Pubns, 1978.

9. Roy, A. E. and Clarke, D., *Astronomy: Principles and Practice*, Institute of Physics Publishing, 2003, pp 133-140.

10. Shuster, M. D., "Stellar aberration and parallax: a tutorial," *Journal of Astronautical Sciences*, Vol. 51, No. 4, 2003, pp. 477–494.